VIROLOGICA SINICA, June 2007, 22 (3):181-192
CLC number: Q786 Document code: A Article ID: 1003-5125(2007)03-0181-12

Expression of Prothrombinase/fibroleukin Gene *fg12* in Lung Impairment in a Murine Severe Acute Respiratory Syndrome Model*

Wei-ming YAN[1], Jia-quan HUANG[2], Xiao-ping LUO[3] and Qin NING[2]**

(*1.Laboratory of Infectious Immunology, 2.Department of Infectious Disease, 3.Department of Pediatrics, Tongji Hospital of Tongji Medical College, Huazhong University of Science & Technology, Wuhan 430030 ,China*)

Abstract: To evaluate the role of murine fibrinogen like protein 2 (mfgl2) /fibroleukin in lung impairment in Severe acute respiratory syndrome (SARS), a murine SARS model induced by Murine hepatitis virus strain 3 (MHV-3) through trachea was established. Impressively, all the animals developed interstitial pneumonia with extensive hyaline membranes formation within alveoli, and presence of micro-vascular thrombosis in the pulmonary vessels. MHV-3 nucleocapsid gene transcripts were identified in multiple organs including lungs, spleen etc. As a representative proinflammatory gene, mfgl2 prothrombinase expression was evident in terminal and respiratory bronchioles, alveolar epithelia and infiltrated cells in the lungs associated with fibrin deposition and micro-vascular thrombosis. In summary, the established murine SARS model could mimic the pathologic characteristics of lungs in patients with SARS. Besides the physical damages due to virus replication in organs, the up-regulation of novel gene mfgl2 in lungs may play a vital role in the development of SARS associated lung damage.

Key words: Severe acute respiratory syndrome (SARS); Murine hepatitis virus strain 3(MHV-3); Lung impairment; Fibrinogen like protein 2 (Fgl2)

Severe acute respiratory syndrome (SARS) is an emerging acute infectious disease with significant morbidity and mortality. The disease is predominantly defined by severe lower respiratory illness and pathological studies of patients who died of SARS showed diffuse alveolar damage in lungs as the most notable feature (1, 6, 11, 13). Treatments of SARS with ribavirin and corticosteroids have not achieved satisfactory results. Furthermore, there is not yet a definite vaccine available for protecting against SARS. A novel virus could be readily isolated from patients' lungs and sputum and cultivated in Vero-E6 cells. Laboratory investigations of such samples using electron microscopy, virus-discovery microarrays containing conserved nucleotide sequences characteristic of many virus families, randomly primed RT-PCR, and serological tests quickly identified that the disease was epidemiologically associated with Severe acute

Received: 2006-10-31, Accepted: 2006-12-25

* Foundation items: National 973 project of Chnia for SARS study (2003CB514112); Ministry of Education of China for SARS study (2003-18); National Science Fund for Distinguished Young Investigators (30225040,. 30123019).

** Corresponding author: Tel/Fax: +86-27-83662391, Email: qning@tjh.tjmu.edu.cn

respiratory syndrome coronavirus (SARS-CoV), an enveloped, positive-stranded RNA virus of the Coronavirade family. Inoculation of monkeys with SARS-CoV caused interstitial pneumonia resembling SARS, and the virus could be isolated from the nose and throat. No viral or bacterial copathogen was needed to induce the disease. These experiments fulfilled Koch's postulates and proved that SARS-CoV is the pathogen of SARS (6, 7, 11, 23, 25). The complete sequences of the virus were deposited in databases and published (17). Phylogenetic analysis of conserved genes of coronaviruses indicates that SARS-CoV is a new branch of coronaviruses and appears more close to the group Ⅱ coronavirus, which includes Bovine coronavirus (BCoV), Murine hepatitis virus (MHV), and Human coronavirus OC43 (HCoV-OC43) (29, 31). MHV can cause fatal systemic diseases in animals. Based upon their initial sites or replication, the MHVs are divided into two major subtypes, respiratory and enteric. Our previous study suggested that in inbred stains of mice, Murine hepatitis virus strain 3 (MHV-3) can produce a clinical syndrome of liver failure similar to that seen in humans through peritoneum, and may be served as an appropriate model to study the pathogenetic mechanisms of fulminant viral hepatitis (21, 26). Though extensive investigations of etiology and pathology of SARS have been reported so far, little information has been gained regarding the mechanisms for the extraordinary virulence of SARS-CoV in human. In this report, we established a murine SARS model with MHV-3 infection through the trachea to investigate the dynamic pathological changes, virus distribution in organs and possible inflammatory factors involved in the disease development, such as murine fibrinogen like protein 2 (mFgl2), a clotting factor and direct prothrombinase, which has been found to play an important role in a variety of diseases characterized by micro-circulation disorders and fibrin deposition (4, 14, 18, 22).

MATERIALS AND METHODS

Mice

All animal studies were carried out according to the guidelines of the Chinese Council on Animal Care and approved by the Tongji Hospital of Tongji Medical School Committees on Animal Experimentation. Female Balb/cJ mice, 6-8 weeks of age, were purchased from Hubei Provincial Institute of Science and Technology, and were housed in individual ventilated cages in the animal facility of Tongji Hospital. Mice were kept in a controlled-temperature (25℃) environment with 12h light-dark cycles and were fed with standard laboratory diet and water. Animals were acclimatized to laboratory conditions for 1 week before experiments and all procedures that involved animals were conducted according to the hospital guidelines.

Virus

MHV-3 was obtained from the American Type Culture Collection (ATCC) and plaque purified on monolayers of DBT cells and titred on L2 cells using a standard plaque assay (12, 16).

Model establishment

To setup the murine SARS model，twenty Balb/cJ mice were inoculated with 100PFU of MHV-3 through trachea. Another twenty Balb/cJ mice injected with sterilized saline through trachea in the same volume were set up as a control. Animal survival rate was then observed. Additionally, 10 Balb/cJ mice were injected

with sterilized saline as a control.

Tissue processing

In a separate experiment, tissues including lungs, spleen, liver, kidneys, intestine, heart, brain were collected at a series of time points from Balb/cJ mice infected with MHV-3 through trachea. The samples were snap freezed and kept at a -80℃ freezer or fixed with 10% formalin for further experiments.

Histological examination

The tissues that had been fixed with 10% formalin were dehydrated in graded alcohol solutions and xylene and embedded in paraffin. 4-μm sections were cut and tissues were then stained with hematoxylin and eosin (HE).

Titration of virus in organs

Approximate 40mg of each frozen organ was homogenized in 0.1 mol/L PBS (pH7.4), and the supernatants were subjected to titer analysis on L2 cells by a standard plaque assay as described elsewhere (12, 16). The titration examination in each organ was repeated for three times in duplicate.

Immunohistochemical staining of mfgl2 prothrombinase

Lungs from Balb/cJ mice infected with MHV-3 through trachea obtained at indicated time points were made into 4-μm paraffin sections to examine the presence of mfgl2. Briefly, tissue sections were dewaxed in xylene and graded alcohol solutions, and then incubated with 3% hydrogen peroxide to quench endogenous peroxidase activity. Microwave heat-induced Ag retrieval in pH6.0 citrate buffer was performed for better staining. An affinity-purified polyclonal Ab against mfgl2 (1:300) was used as the primary Ab, which was produced in rabbits by repeated injections with a 14-aa hydrophilic peptide (CKLQADDHRDPGGN) from exon 1 of the mfgl2 prothrombinase. A standard streptavidin-biotin amplification system was involved in detection of mfgl2 (18). As a negative control, a rabbit IgG was used as the primary Ab instead of a specific Ab. A parallel mfgl2 detection was also performed on tissue sections from the sterilized saline injected Balb/cJ mice as a experimental control.

***In situ* hybridization(ISH) analysis**

MHV-3 oligonucleotide probes: Two oligonucleotide probes were synthesized according to the published nucleocapsid gene sequence of MHV-3 coronavirus. The sequences were 5′-AAGAGAATG AATCCTATGTCGGCGCTCGGT-3′ (nt1365-1394) and 5′-TCCAACCAGCGCCAGCCTGCCTCTACT GTA-3′ (nt658-687). Both of the probes were enzymatically labeled at their 3'-ends with terminal transferase by incorporation of a single digoxigenin-labeled dideoxyuridine-triphosphate (DIG-ddUTP) (Roche, Germany Cat.No.3353575).

mfgl2 cDNA probe: A 169-bp DNA fragment from the carboxyl end of the mfgl2 coding region in exon 2 was used as a template to synthesize anti-sense digoxigenin-11-UTP-labeled cDNA probes. The probes were labeled with digoxigenin according to the randomly primed labeling technique (Roche, Germany Cat.No.1745832). The sensitivity and specificity of the probes were determined by dot blotting analysis (data not shown).

ISH: All ISH were performed on paraffin wax-embedded tissue sections as described before (18). The oligonucleotide probe for nucleocapsid gene of MHV-3 was used in 30pmol/mL concentration. The cDNA probe for mfgl2 was used in 2.5μg/mL concentration.

Double immunochemistry staining analysis

To histologically visualize the association of mfgl2 expression with fibrin deposition, a double immunochemistry staining was performed, in which standard streptavidin-biotin amplification system was used. A rabbit polyclonal Ab against mfgl2 (1:300) and a rabbit polyclonal Ab against fibrin (DAKO, Denmark Code No.A0080, Lot 097) (1:600) were used as primary antibodies respectively. Two distinct substrate/chromogen/enzyme systems were used to show two distinct antigens. BCIP/NBT/alkaline phosphatase system, which produces a dark purple colour, indicated mfgl2 expression. While hydrogen peroxide/AEC/peroxidase, which produces an intense red colour, indicated fibrin deposition.

Statistical analysis

Quantitative data were reported as the means ± standard deviation for at least three separate experiments. Differences of virus titers between organs at 48h following MHV-3 infection were analyzed by using one-way analysis of variance, and a P value of less than 0.05 was considered statistically significant.

RESULTS

Survival rate

Balb/cJ mice inoculated with MHV-3 through trachea began to develop a wasting syndrome at 24h post infection characterized by weight loss, alopecia, oily hair and paralysis. All mice died within 5 days as shown in Fig. 1. While Balb/cJ mice injected with the same volume of sterilized saline in the control group did not show any clinical manifestation and survived until an observation time of one month post injection.

Histopathological findings

In a separate set of experiment, tissues including lungs, spleen, liver, kidneys, intestine, heart and brain from Balb/cJ mice infected with MHV-3 through trachea were examined as described above. Various histopathological changes were found in these organs (shown in Fig.2 and Fig.3).

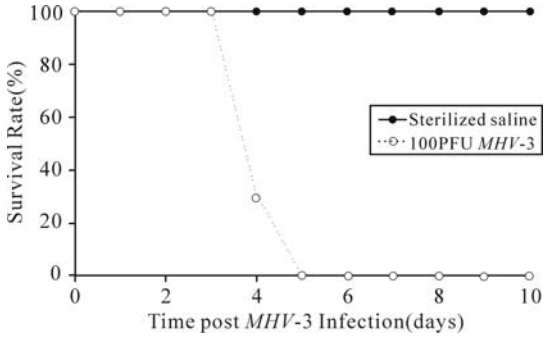

Fig. 1. The survival rate of Balb/cJ mice inoculated with MHV-3 through trachea. When twenty Balb/cJ mice were challenged with 100PFU of MHV-3 through trachea, all animals died within 5 days (…○…), while the control mice injected with the same volume of sterilized saline survived until an observation time of one month post injection (—●—).

Lungs: The lungs displayed red color with areas of atrophy on the surface. As the infection progressed, the microscopic pathological features were dominated by diffuse alveolar septum thickness with numerous lymphocytes and mononuclear cells inflammatory infiltrates at 72h to 96h post infection. A mixture feature of serosity, protein exudates and hemorrhagic inflammation were seen in most pulmonary alveoli with engorgement of capillary (Fig.2. A1-A4). Microthrombosis could be easily observed in accompanied vessels (Fig.2. A5). Extensive hyaline membrane formation in alveoli is another typical pathological featurein the infected lungs (Fig.2. A6). No typical multinucleated syncytial cells were observed within the lung sections.

Spleen: The damages of the spleen under the microscope included the reduction of lymphocytes around the lymphatic sheath, focal hemorrhage and

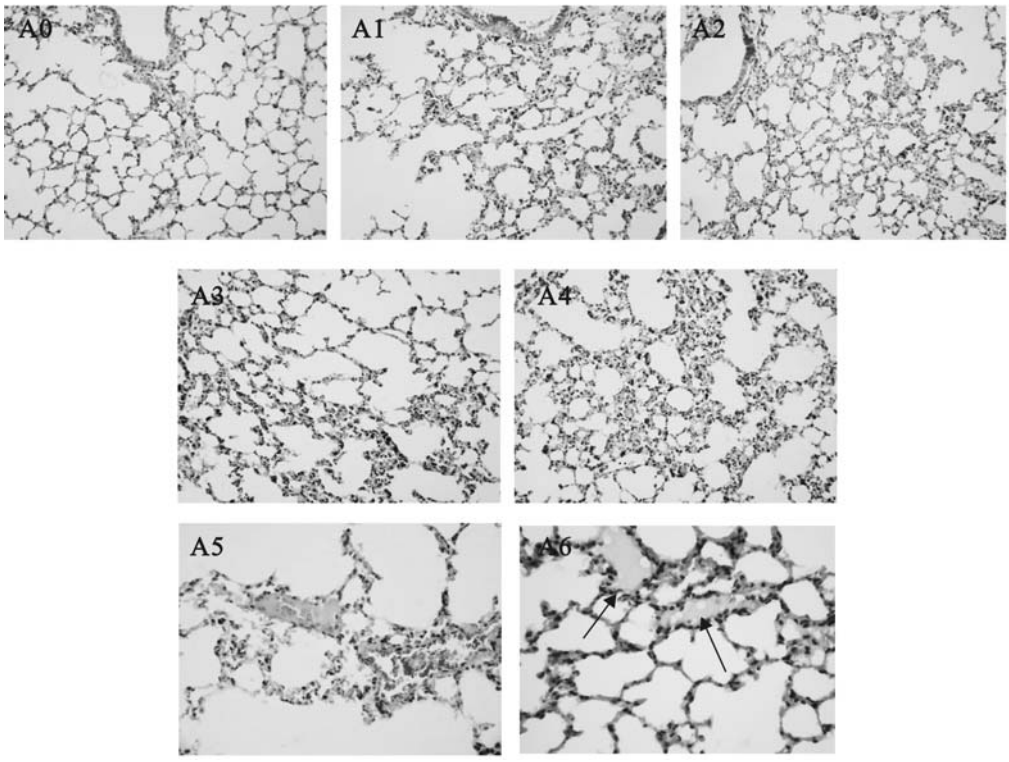

Fig.2. Histological examinations in lungs from Balb/cJ mice infected with MHV-3 through the trachea by H&E staining. Panel A0: lungs from sterilized saline injected control animals; Panel A1, A2, A3, A4: lungs at 24h to 96h post MHV-3 infection; Panel A5: some fibrous thrombosis in the accompanied vessels; Panel A6: hyaline membrane formation in alveoli .

congestion near the capsule. Massive patchy necrosis of splenic lymphoid tissue could be observed at 96h following MHV-3 infection as shown in Fig.3. A4 .

Liver: Infected liver tissues showed widespread cloudy swelling, prominent ballooning degeneration with mild lymphocytic infiltration in the portal area. Dot and zonal hepatocellular necrosis could only be found occasionally at 96h post MHV-3 infection (Fig.3. B4).

Kidneys: The cortices of kidneys were thinner. Most of the glomeruli appeared normal, with occasionally localized hemorrhage. A few renal tubules displayed hydropic degeneration or swelling and had some protein casts as shown in Fig.3.C4.

Intestine, heart and brain: No significant pathological changes were found in these organs (Fig.3. D4, E4, F4).

Viral titers and virus distribution

To determine viral titers, tissues were homogenized and the supernatants were subjected to titer determination on L2 cells as described previously (12, 16). Virus plaques were found in all collected organs and increased with the progress of the infection (shown in Fig.4). Virus titers increased in all collected tissues from 24 h to 96h post infection. P values to indicate the differences of virus titers among different tissues at 48h following MHV-3 infection were measured and displayed that viral titers in the lungs, spleen, liver were significantly higher than those in other organs ($P<0.05$). There were no difference in viral titers between tissues of lungs and spleen, kidneys and brain, intestine and heart ($P>0.05$).

Since the presence of MHV-3 in organs from the murine SARS model was confirmed by the virus

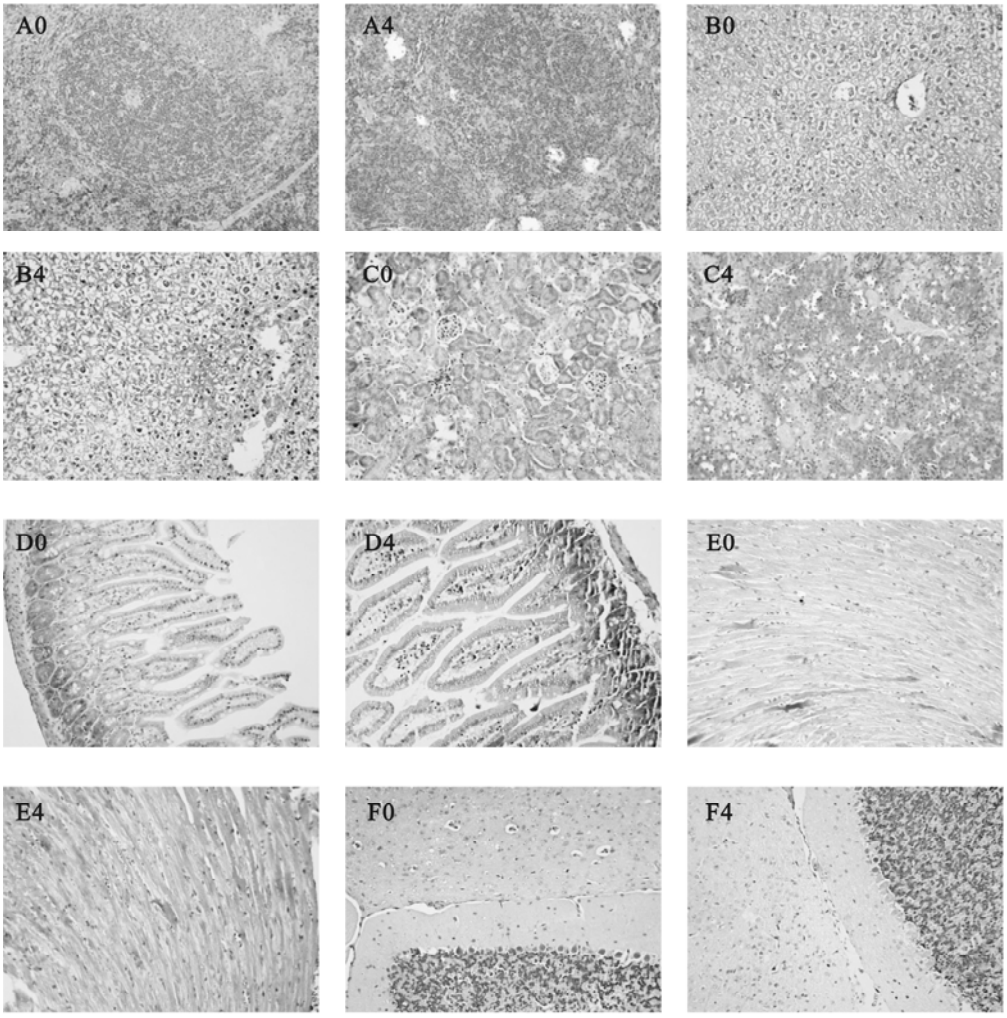

Fig. 3. Histological examinations in other organs from Balb/cJ mice infected with MHV-3 through the trachea by H&E staining.Panel A0, B0, C0, D0, E0, F0: spleen, liver, kidneys, intestine, heart and brain from sterilized saline injected control animals; Panel A4, B4, C4, D4, E4, F4: spleen, liver, kidneys, intestine, heart and brain at 96h post MHV-3 infection .

plaque analysis described above, we further detected the MHV-3 nucleocapsid gene fragment by the ISH technique in these organs in order to investigate the MHV-3 targeted cells. As shown in Fig.5, MHV-3 nucleocapsid gene transcripts were detected predominantly in the cytoplasm of alveolar epithelia, serous gland epithelia of the trachea/bronchus, infiltrated lymphocytes in the lungs, cells distributed at the periphery of the germinal centers in the spleen, hepatocytes, epithelia of the distal renal tubules, epithelia of intestine, myocardial cells and cerebral neurons.

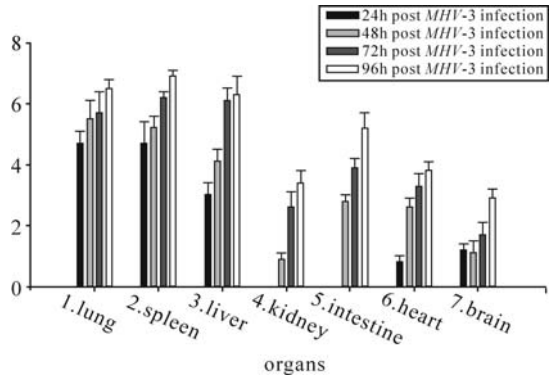

Fig. 4. Determination of viral titers in organs in Balb/cJ mice infected with MHV-3 through the trachea. *P* values to indicate the differences of virus titers among different tissues at 48h following MHV-3 infection were measured and displayed that viral titers in the lungs, spleen, liver detected were significantly higher than those in other organs ($P<0.05$). There were no difference in viral titers between tissues of lungs and spleen, kidneys and brain, intestine and heart ($P>0.05$).

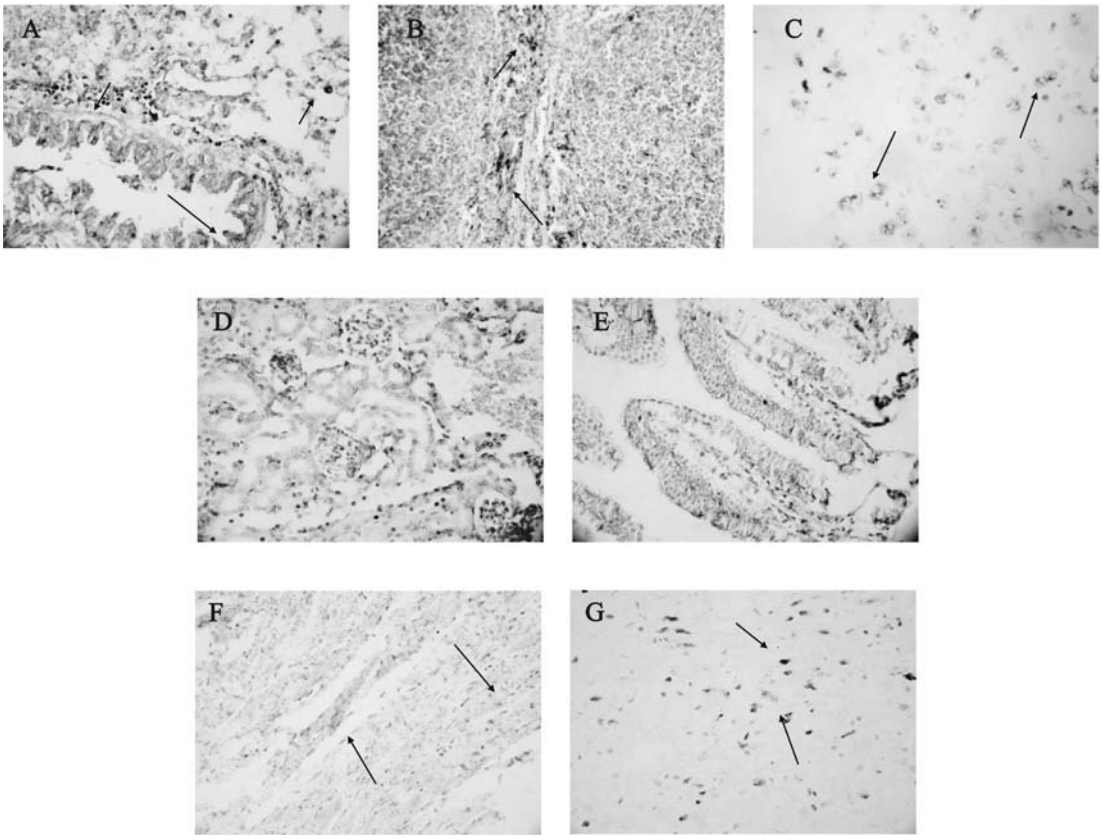

Fig. 5. Detection of the MHV-3 nucleocapsid gene fragment in organs from Balb/cJ mice infected with MHV-3 through the trachea by ISH. Panel A, B, C, D, E, F, G: MHV-3 nucleocapsid gene transcript in the lungs, spleen, liver, kidneys, intestine, heart and brain. The dark purple colour in cells(arrow) represents positive signal for MHV-3 nucleocapsid gene transcripts.

mfgl2 expression in lungs

mfgl2 protein expression in lungs: As shown in Fig 6 panel A, the strong positive staining of mfgl2 protein could be found mainly in the cytoplasm of terminal and respiratory bronchioles, alveolar epithelia and infiltrating cells in the lungs. In sterilized saline injected Balb/cJ mice, there was a weak elementary staining of mfgl2 in lungs. The absence of specific brownish-yellow colour in the MHV-3 infected organs using rabbit IgG as the primary Ab suggested the specificity of the polyclonal Ab against mfgl2 prothrombinase.

mfgl2 mRNA expression in lungs: Detection of mfgl2 transcripts was focused in lungs post infection (Fig.6. B1-B3). mfgl2 mRNA transcripts were evident in the cytoplasm of the terminal and respiratory bronchioles, alveolar epithelia and infiltrated cells in the lungs.

Double staining analysis

Widespread fibrin deposition in association with the mfgl2 expression, especially in microvasculars (Fig.7. A) and hyaline-membranes (Fig.7. B) was detected in the lungs.

DISCUSSION

As we know, an ideal animal model is important to the progress of SARS research. Previous studies indicate that the Golden Syrian hamster infected with SARS-CoV has a higher virus replication, a longer duration in the respiratory tract and is accompanied by

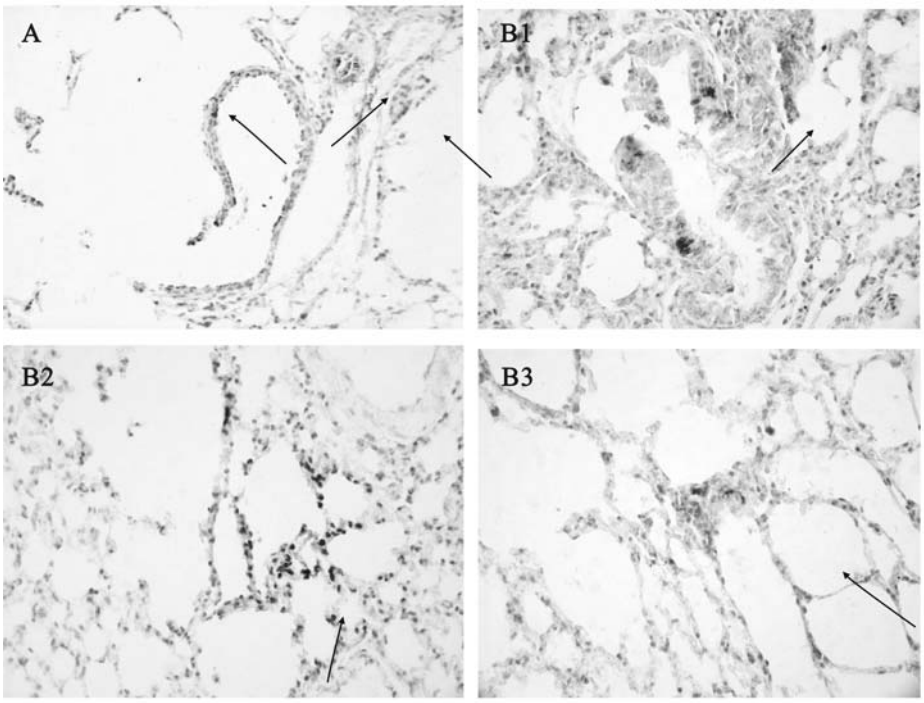

Fig. 6. Immunohistochemical and ISH detection of mfgl2 expression in lungs from Balb/cJ mice infected with MHV-3 through the trachea. Panel A: mfgl2 protein expression in the lungs. The brownish-yellow colour in cells(arrow) represents positive signal for mfgl2 protein expression; Panel B1, B2, B3: mfgl2 transcripts in cytoplasm of terminal and respiratory bronchioles, alveolar epithelia, and infiltrating cells in stroma. The dark purple colour in cells(arrow) represents positive signal for mfgl2 transcripts.

significant pathological changes, but showed no evidence of the disease (27). Though primates have been confirmed to be optimal animal model for human SARS study, the expense and rarity of the animal obviates their use by most research institutes. The accompanying environmental requirements for the use of a biosafety level 4 laboratory is another obstacle to its widespread study, given the serious nature of SARS-CoV and the evidence of the person-to-person transmission pathway. Even so, many primates failed to mimic characters of SARS disease well. When rhesus and cynomolgus macaques were challenged

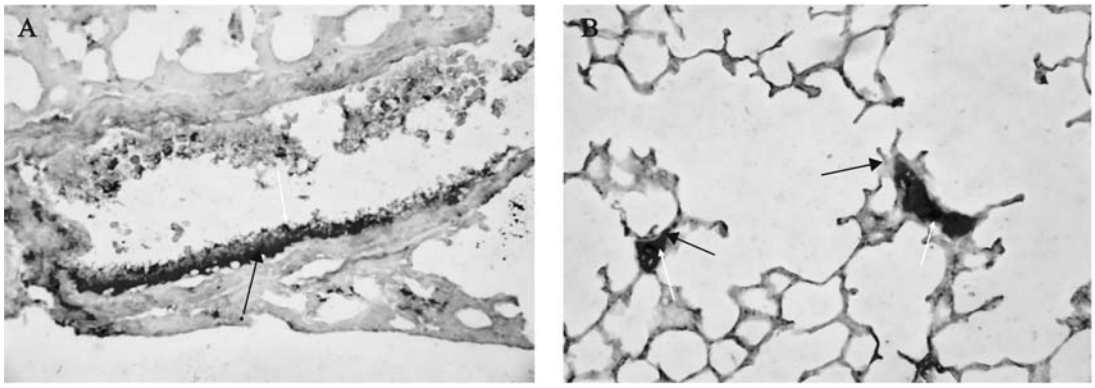

Fig. 7. The co-localization of mfgl2 and fibrin detected by double immunochemistry staining. Widespread fibrin deposition around where mfgl2 expressed, especially in microvasculars (panel A) and hyaline-membranes (panel B) were detected in the lungs. The dark purple staining indicated mfgl2 expression(yellow arrow), while intense red staining indicated fibrin expression(blue arrow) .

with 10^7 PFU SARS-CoV, some of the animals developed a mild self-limited respiratory infection, very different from what observed in patients with SARS (28). McAuliffe and colleagues (19) also noticed that though moderate to high titers of SARS-CoV with associated interstitial pneumonitis could be detected in the lungs of African Green monkeys on day 2 and have been resolved by day 4 post-infection, virus replication was highly restricted and there was no evidence of enhanced disease 2 months later. Taken together, although these models will be useful for the evaluation of immunogenicity of candidate vaccines, the lack of apparent clinical illness and variability from animal to animal in the level of viral replication result in their limited usefulness in the study of SARS and the evaluation of therapeutic effects.

Given that small animal models are urgently needed, we established a murine SARS model, in which Balb/cJ mouse, a standard laboratory rodent was involved. Previous study has indicated that significant pathological features were absent, though SARS-CoV replication was evident in mice (10). Instead of SARS-CoV, we infected Balb/cJ mice with MHV-3, a member of the group Ⅱ coronavirus. Significantly, we found that animals died from a multiple organ dysfunction disease in 5 days post MHV-3 infection. As described in our results, although many organs were involved, the predominant damage was restricted to lungs. Other atypical pathological changes, such as mild hydropic degeneration, interstitial cell proliferation and dot necrosis could occasionally be detected in spleen, liver and kidneys. The pathological features displayed here is in consistent with reports from the experience with SARS patients (5, 11, 13, 25, 33).

More recently in vitro evidence also suggests that SARS-CoV may have infected human cells derived from lungs, kidneys, liver, and intestine (9). Beside the respiratory distress, other clinical symptoms in SARS patients also supported the conclusion that virus could attack many organs in an infected individual. For example, liver impairment was commonly reported in up to 60%-66% of patients with SARS (2, 32-34). In addition, the virus replication found in renal tubular epithelial cells and the crypt epithelial of intestine suggested that these were two possible transmission pathways of SARS-CoV. In our study, we also detected virus in all collected organs from Balb/cJ mice infected with MHV-3 through trachea with a significantly higher level in lungs, spleen and liver when compared with those in kidneys, intestine, heart and brain.

Nucleocapsid protein of coronavirus is the key protein for the formation of the helical nucleocapsid during virion assembly. The nucleocapsid protein is also immunogenic and abundantly expressed during infection, and believed to be more conserved than other proteins of the virus, such as spike and membrane glycoproteins. Therefore, it has been widely used as an important viral Ag in immuno-logical and immunohistochemical assays for clinical diagnosis and laboratory detection of coronavirus infection (15, 35). In order to determine the virus targeted cells post inoculation of MHV-3 through trachea in Balb/cJ mice, we detected the nucleocapsid gene transcripts in collected tissues by ISH, in which two oligonucleotide probes were designed according to nucleocapsid gene sequence. Both probes were combined to ensure sensitivity and specificity of the detection. The results revealed that MHV-3 could

target a variety of cells post infection as described in the results, which was consistent with what has been reported in SARS patients (3, 30).

Of particular relevance to this report is the extensive studies of the pathogenesis of fulminant viral hepatitis using the same virus in Balb/cJ mice but infected through a different pathway, through the peritoneum instead of trachea (3, 30). Although the virus replication and distribution were shown similar patterns in both animal models, the pathological features in different organs especially lungs, liver and spleen were significantly different. In Balb/cJ mice infected with MHV-3 through peritoneum, the damage within liver is massive and fatal, characterized by widespread necrosis of hepatocytes within 48-72h and all animals have died by 72h with only mild or no disorder in other organs such as lungs and spleen (4). In Balb/cJ mice infected with MHV-3 through the trachea, animals died up to 120h post infection with widespread injury, especially in lungs, characterized by diffuse thickened alveoli septums with numerous lymphocytes and mononuclear cells inflammatory infiltrates, extensive hyaline membrane in pulmonary alveoli, engorgement of capillary or microthrombosis in accompanied vessels at 72h to 96h post infection. However, even by 96h post infection, the damage in liver was still mild, characterized by cloudy swelling, prominent ballooning degeneration with mild lymphocytic infiltration in the portal area and occasionally dot or zonal hepatocyte necrosis. We further measured the serum alanine aminotransferase (ALT) level at 48h post MHV-3 infection to show the liver function within both models. The results displayed that the ALT level (945.8 ± 32.2 IU/L) in Balb/cJ mice infected with MHV-3 through peritoneum is sevenfold as high as that(112.7±36.5 IU/L) in Balb/cJ mice infected with MHV-3 through trachea with the ALT level of 39±2.94IU/L in saline injected Balb/cJ mice (detail data not shown), indicating that instead of fulminant liver failure, severe lesion in lungs and disreputed host immune system were the fetal cause of the Balb/cJ mice when infected with MHV-3 through trachea. Since both the infectious pathway and the pathological features in this murine SARS model induced by MHV-3 through trachea in Balb/cJ mice mimic those in human with SARS-CoV infection, the murine SARS model therefore could provide an attractive and convenient system for the dynamic pathophysiology investigation in SARS-CoV infection.

Although the viral titers in lungs, spleen, liver where disease displayed were significantly higher than those in other organs such as kidneys and brain, there were still a large amount of virus harvested from tissues with only mild or no pathologic disorders, suggesting that in addition to cytopathic effect (CPE) mediated by local virus replication, host factors contributed greatly to the pathologic injury. To date, the details of the host response to SARS-CoV infection is still largely unknown and consequently the most appropriate treatment regime remains to be established. A human peripheral blood mononuclear cells model system was established by Genome Institute of Singapore to investigate genome-wide host responses to SARS-CoV infection (20), while detailed *in vivo* studies of the host response are now required. Data from our and other laboratories have suggested that host factors may be another important factor in the pathogenesis of MHV-3 disease (26), herein a murine SARS model was used to investigate the host

response *in vivo* and as a proinflammatory gene. fgl2/fibroleukin is an immune coagulant, which can bypass the TF/factorⅦ extrinsic pathway and directly cleave prothrombin to thrombin, followed by fibrin deposition and thrombosis formation. Though having the characteristics of a serine protease, mfgl2 immunoactivity is not inhibited by antithrombin III (4). Evidence showed that mfgl2 has an important role in many diseases, such as fulminant viral hepatitis (14, 18), syngeneic transplantation (22) and fetal loss syndrome, whose pathogenesis was dominated by thrombosis in the microvasculature. Since patients dying from SARS revealed the presence of vascular thrombosis in pulmonary vessels (8, 24, 25), we investigated the role of mfgl2 in the lung impairment of murine SARS by Balb/cJ mice infected with MHV-3 through trachea. In our study, specific mfgl2 transcripts and immunoreactive protein were seen in the cytoplasm of terminal and respiratory bronchioles, most of the alveolar epithelia and infiltrating cells in the stroma. Double immunochemistry staining revealed widespread fibrin deposition in association with mfgl2 expression in lungs, especially within the vessels and hyaline-membranes. Therefore fibrin induced by mfgl2 from alveolar epithelia is considered to be involved in this process. In a similar way, specific co-localization of mfgl2 and fibrin in microvasculars, in addition to accumulation of numerous erythrocytes indicated the activation of coagulation system induced by mfgl2. Hyaline-membranes appear to be a pivotal mediator in acute respiratory distress, while thrombin can target the vascular endothelial cells and induce secretion of proinflammatory mediators and adhesion of leukocytes, which together potentiate the inflammatory response. Therefore our data provides new insight into the importance of mfgl2 in the lung impairment in MHV-3 induced murine SARS. These findings warrant further investigation of human fibrinogen like protein 2 (hFgl2) expression in patients with SARS. If host factors such as Fgl2 play an important role in SARS progression, a new logical target for molecular manipulation can be investigated and will offer hope for development of new treatment approaches for patients with SARS.

References

1. **Booth C, Matukas L, Tomlinson G.** 2003. Clinical features and short-term outcomes of 144 patients with SARS in Toronto Area. **JAMA,** 289: 2801-2809.
2. **Chau T, Lee K, Yao H.** 2004. SARS-associated viral hepatitis caused by a novel coronavirus: report of three cases. **Hepatology,** 39: 302-310.
3. **Chow K, Hsiao C, Lin T.** 2004. Detection of severe acute respiratory syndrome-associated coronavirus in pneumocytes of the lung. **Am J Clin Pathol,** 121: 574-580.
4. **Ding J, Ning Q, Liu M.** 1997. Fuliminant hepatic failure hepatitis virus strain 3 infection: tissue-specific expression of a novel fgl2 prothrombinase. **J Virol,** 71: 9223-9230.
5. **Ding Y, Wang H, Shen H, *et al.*** 2003. The clinical pathology of severe acute respiratory syndrome (SARS): a report from China. **J Pathol,** 200 (3): 282-289.
6. **Drosten C, Gunther S, Preiser W, *et al.*** 2003. Identification of a novel coronavirus in patients with severe acute respiratory syndrome. **N Engl J Med,** 348 (20): 1967-1976.
7. **Fouchier R, Kuiken T, Schutten M**. 2003. Aetiology: Koch's postulates fulfilled for SARS virus. **Nature,** 423: 240.
8. **Franks T, Chong P, Chui P.** 2003. Lung pathology of severe acute respiratory syndrome (SARS): a study of 8 autopsy cases from Singapore . **Hum Pathol,** 34: 743-748.
9. **Gillim-Ross L, Taylor J, Scholl D R, *et al.*** 2004. Discovery of novel human and animal cells infected by the severe acute respiratory syndrome coronavirus by replication-specific multiplex reverse transcription-PCR. **J Clin Microbiol,** 42 (7): 3196-3206.
10. **Glass W, Subbarao K, Murphy B.** 2004. Mechanisms of

host defense following severe acute respiratory syndrome-coronavirus (SARS-CoV) pulmonary infection of mice. **J Immunol**, 173: 4030-4039.

11. **Ksiazek T, Erdman D, Goldsmith C.** 2003. A novel coronavirus associated with severe acute respiratory syndrome. **N Engl J Med,** 348: 1953-1966.
12. **Lamontagne L, Jolicoeur P.** 1991. Mouse hepatitis virus 3-thymic cell interactions correlating with viral pathogenicity. **J Immunol,** 146 (9): 3152-3159.
13. **Lee N, Hui D, Wu A.** 2003. A major outbreak of severe acute respiratory syndrome in Hong Kong. **N Engl J Med,** 348: 1986-1994.
14. **Levy G, Liu M, Ding J.** 2000. Molecular and functional analysis of the human prothrombinase gene (HFGL2) and its role in viral hepatitis. **Am J Pathol**, 156: 1217-1225.
15. **Lin Y, Shen X, Yang R.** 2003. Identification of an epitope of SARS-coronavirus nucleocapsid protein. **Cell Res,** 13: 141-145.
16. **MacPhee P, Dindzans V, Fung L.** 1985. Acute and chronic changes in the microcirculation of the liver in inbred strains of mice following infection with mouse hepatitis virus type 3. **Hepatology,** 5: 649-660.
17. **Marra M, Jones S, Astell C.** 2003. The genome sequence of SARS-associated coronavirus. **Science,** 300: 1399-1404.
18. **Marsden P, Ning Q, Fung L.** 2003. The fgl2/fibroleukin prothrombinase contributes to immunologically mediated thrombosis in experimental and human viral hepatitis. **J Clin Invest,** 112: 58-66.
19. **McAuliffe J, Vogel L, Roberts A, *et al.*** 2004. Replication of SARS coronavirus administered into the respiratory tract of African Green, rhesus and cynomolgus monkeys. **Virology,** 330 (1): 8-15.
20. **Ng L, Hibberd M, Ooi E.** 2004. A human in vitro model system for investigating genome-wide host responses to SARS coronavirus infection. **BMC Infect Dis, 4**: 34.
21. **Ning Q L X, Yan WM.** 2004. A method to establish a murine model of fulminant viral hepatitis [Patent]. China.
22. **Ning Q, Sun Y, Han M.** 2005. Role of Fgl2 Prothrombinase/ Fibroleukin in Experimental and Human Allograft Rejection. **J Immunol,** 174: 7403-7411.
23. **Osterhaus A, Fouchier R, Kuiken T.** 2004. The aetiology of SARS: Koch's postulates fulfilled. **Philos Trans R Soc Lond B Biol Sci**, 359: 1081-1082.
24. **Peiris J, Chu C**, **Cheng V.** 2003. Clinical progression and viral load in a community outbreak of coronavirus-associated SARS pneumonia: a prospective study. **Lancet,** 361: 1767-1772.
25. **Peiris J, Lai S, Poon L.** 2003. Coronavirus as a possible cause of severe acute respiratory syndrome. **Lancet,** 361: 1319-1325.
26. **Pope M, Rotstein O, Cole E, *et al.*** 1995. Pattern of disease after murine hepatitis virus strain 3 infection correlates with macrophage activation and not viral replication. **J Virol,** 69: 5252-5260.
27. **Roberts A, Vogel L, Guarner J, *et al.*** 2005. Severe acute respiratory syndrome coronavirus infection of golden Syrian hamsters. **J Virol,** 79 (1): 503-511.
28. **Rowe T, Gao G, Hogan R.** 2004. Macaque model for severe acute respiratory syndrome. **J Virol,** 78: 11401-11404.
29. **Snijder E, Bredenbeek P, Dobbe J.** 2003. Unique and conserved features of genome and proteome of SARS-coronavirus, an early split-off from the coronavirus group 2 lineage. **J Mol Biol,** 331: 991-1004.
30. **To K, Tong J, Chan P.** 2004. Tissue and cellular tropism of the coronavirus associatedwith severe acute respiratory syndrome: an in-situ hybridization of fatal cases. **J Pathol**, 202: 157-163.
31. **Wu S, Du C, Wan P.** 2003. The genome comparison of SARS-CoV and other coronaviruses. **Hereditas (Beijing),** 25: 373-382. (in Chinese)
32. **Yin C, Wang C, Tang Z.** 2004. Clinical analysis of multiple organ dysfunction syndrome in patients suffering from SARS. **Chin Critica1 Care Med,** 16: 646-650. (in Chinese)
33. **Zhang J.** 2003. Severe acute respiratory syndrome and its lesions in digestive system. **World J Gastroenterol**, 9: 1135-1138.
34. **Zhao L, Xing H, Xu L.** 2004. Effect of SARS-associated coronavirus on peripheral blood picture and liver function. **Chin Critica1 Care Med,** 16: 660-663. (in Chinese)
35. **Zhao P, Cao J, Zhao L.** 2005. Immune responses against SARS-coronavirus nucleocapsid protein induced by DNA vaccine. **Virology,** 331: 128-135.